Ocean Modelling 40 (2011) 133–146

Contents lists available at SciVerse ScienceDirect

Ocean Modelling

journal homepage: www.elsevier.com/locate/ocemod

Establishment of momentum balance by form stress in a wind-driven channel

Marshall L. Ward *, Andrew McC. Hogg

Research School of Earth Sciences, Australian National University, Canberra, ACT 0200, Australia

ARTICLE INFO

Article history:
Received 20 November 2010
Received in revised form 24 July 2011
Accepted 7 August 2011
Available online 22 August 2011

Keywords:
Channel flow
Wind-driven currents
Momentum transfer
Mesoscale eddies
Ekman transport
Modelling

ABSTRACT

We examine the establishment of form stress in the spinup of a rotating isopycnal wind-driven channel model, with reference to the Antarctic Circumpolar Current. Initially, the force balance resembles Ekman layer transport, where zonal surface winds are balanced by the Coriolis forces in the upper layers, while the bottom layers consist of an opposing meridional flow balanced by topographic form stress. As the meridional transport increases, the isopycnal slopes and zonal transport also increase and the flow becomes baroclinically unstable, leading to the development of interfacial form stresses due to small-scale baroclinic eddies. This form stress alters the force balance of the layers, causing the system to geostrophically readjust to new states with progressively lower meridional transports. This trend continues until the meridional transport stops and the current is balanced solely by winds and form stress. The final state is a turbulent flow consisting of a several meandering jets that are maintained by the mesoscale eddy field. Our results resemble recent observations of the Antarctic Circumpolar Current and illustrate the contribution of mesoscale eddies to the force balance of the Southern Ocean.

1. Introduction

The currents of the Southern Ocean, from the Antarctic Circumpolar Current (ACC) to its smaller scale features, are dynamically distinct from the large-scale circulations that characterise most of the world's oceans. The Southern Ocean is the only circumpolar ocean, and therefore the only one that can support balanced, coherent transport along contours of constant planetary potential vorticity (PV). Measurements across Drake Passage indicate transports of approximately 140 Sv (Cunningham et al., 2003) ($1\ \mathrm{Sv} \equiv 10^6\ \mathrm{m^3\ s^{-1}}$), and altimetric observations confirm the existence of several narrow zonal jets along sharp isopycnal slopes in the Southern Ocean (Sokolov and Rintoul, 2007). The locations of the jets exhibit strong meridional fluctuations, such as meanderings of several degrees of latitude within an environment of energetic mesoscale eddies up to 100 km in size. Surface geostrophic velocities can reach values on the order of $1\ \mathrm{m\ s^{-1}}$, leading to a strongly inertial environment whose large-scale properties are connected to the behaviour of small-scale structures.

There have been several theories describing the mean circulation and zonal transport of the ACC. Circulation theories based on Sverdrup transport provide comparable estimates to observed transports (Stommel, 1957), but the predicted transports depend directly on the wind stress curl and are defined by the background planetary PV field, even though observed flows clearly contain strong relative vorticity fields. Despite the apparent prevalence of strong nonlinear features, there have been notable efforts to reconcile these differences (Hughes, 2002; Nadeau and Straub, 2009), but it seems evident that steady solutions based on Sverdrup transport alone cannot reproduce the dynamic structure of a realistic Southern Ocean circulation.

Alternative theories draw upon an early suggestion by Munk and Palmén (1951), who observed that a periodic channel resembling the Southern Ocean and driven by representative surface winds could only be balanced by lateral dissipative processes for transports of at least 1000 Sv, if not larger, which greatly exceed observations. They propose instead that surface winds are balanced by topographic form stress from Southern Ocean bathymetry, which restricts the transport to a more observationally consistent value. Early numerical modelling confirmed these ideas, where models with flat bottoms either produced excessive zonal transport (Hidaka and Tsuchiya, 1953) or required prohibitively large viscous parameters to produce realistic transports (Gill and Bryan, 1971).

Quasigeostrophic modelling studies, which can accurately resolve small-scale dynamics at the cost of restricting the displacement of isopycnal interfaces to small amplitude, have successfully reproduced many of the features described above when forced by analogous Southern Ocean winds and bathymetry, such as a net zonal transport constrained by topographic form stress (McWilliams et al., 1978; Treguier and McWilliams, 1990; Wolff et al., 1991) and quasi-steady zonal jets sustained by mesoscale eddies (Hogg and Blundell, 2006; Thompson, 2010). The momentum in these models is transported from the surface to the bottom by

* Corresponding author.
E-mail addresses: marshall.ward@anu.edu.au (M.L. Ward), andy.hogg@anu.edu.au (A.M. Hogg).

1463-5003/$ - see front matter © 2011 Elsevier Ltd. All rights reserved.
doi:10.1016/j.ocemod.2011.08.004

interfacial form stress, which transfers momentum between density layers by mesoscale eddies. Other eddy permitting (but still highly parameterised) studies have reached similar conclusions (Killworth and Nanneh, 1994).

Many of these quasigeostrophic studies have been disputed, however, due to their inability to support diapycnal exchange and an overturning circulation (Warren et al., 1996). It has been proposed that an induced overturning circulation or the transport of heat by mesoscale eddies sets the zonal transport through modification of the background stratification (Karsten and Marshall, 2002; Marshall and Radko, 2003). However, mesoscale eddies remain a significant factor in such models, whose interfacial form stress cannot be dismissed entirely (Hallberg and Gnanadesikan, 2001, 2006).

Despite the objections to wind-driven channel models of the Southern Ocean, it is evident that a circulation over bathymetry will subject the ocean to form stress, and that such forces must be considered in any momentum balance of the Southern Ocean (Olbers, 1998; Olbers et al., 2004). Johnson and Bryden (1989) demonstrated that a simple model for the balance between wind stress and interfacial form stress is capable of producing observationally consistent transport estimates. Straub (1993) presented conceptual arguments for the emergence of interfacial form stress, whereby elevated levels of wind stress preferentially produce eddies via baroclinic instability rather than accelerated transport, which has been supported in high-resolution numerical simulations (Meredith and Hogg, 2006; Hogg et al., 2008; Screen et al., 2009). Several theories of wind-driven transport were tested by Tansley and Marshall (2001) in a two-layer geostrophic model. They found that the zonal transport in an idealised wind-forced channel was best characterised by the relationship between wind stress, rather than wind stress curl, but that no single proposed theory was capable of reproducing the sensitivity of the transport to the wind stress.

These issues highlight one of the major difficulties in understanding Southern Ocean dynamics. There are many competing theories explaining the ocean circulation in this region, but no clear method of falsifying them if several mechanisms contribute to the dynamics of the observed current. The Southern Ocean remains a poorly constrained component of large-scale climate models (Russell et al., 2006) and it is still not clear which processes must be parameterised or resolved in order to produce a realistic circulation in Southern Ocean models. While most parameterisations can often be tuned to produce an approximately valid transport, they rarely guarantee an accurate reproduction of the response to changes in external forcing. A more detailed physical understanding of each of these mechanisms is therefore necessary if we are to skilfully emulate the future behaviour of the Southern Ocean.

In this paper, we describe the spinup of a zonally re-entrant numerical model forced by surface winds, with an emphasis on the force balance of individual isopycnal layers. In particular, we discuss the emergence of interfacial form stress applied to the layers by mesoscale eddies. We find that equilibrium does not require a coherent southward eddy transport to balance the northward Ekman transport. Instead, the mesoscale eddy field modulates the Ekman transport by the formation of interfacial form stress. We also find that mesoscale eddies are not required to transmit momentum from the surface to the bathymetry, and that the momentum balance is preserved through geostrophic adjustment. The model evolves through several dynamical regimes during spinup, characterised by the gradual recession of Ekman transport and emergence of interfacial form stress, and equilibrium is established after the interfacial form stress matches the surface wind forcing at every level. Section 2 describes the numerical model and quantitative methods used to determine the interfacial form stress in each isopycnal layer. Section 3 presents time series for the zonal transport of the channel, as well as the forces applied to each layer during spinup. This is followed by zonally averaged profiles of the forces across the channel at distinctive stages of spinup, including a discussion of the dynamic structure of the flow at each stage. Section 4 highlights our major results and considers the implications for the ACC and the Southern Ocean.

2. Methods

2.1. Model

In this study, we use the isopycnal ocean model of Hallberg and Gnanadesikan (2006), which is a recent adaptation of the Hallberg Isopycnal Model (Hallberg, 1995). The domain is a zonally re-entrant channel of length $L_x = 5120$ km and width $L_y = 2560$ km and a maximum depth of 4000 m, with vertical free-slip walls along the north and south boundaries. The stratification consists of five adiabatic layers, prescribed in Table 1. For the stratification shown, the largest baroclinic deformation radius at initialisation is $\lambda_1 = 30$ km. The grid resolution is $\Delta x = 6.4\ \text{km} \approx 0.2\lambda_1$, ensuring that we have an eddy-resolved isopycnal flow. Background rotation is β-plane, and we use comparative Southern Ocean values of $f_0 = -10^{-4}\ \text{s}^{-1}$ and $\beta = 1.5 \times 10^{-11}\ \text{m}^{-1}\ \text{s}^{-1}$ where f_0 is the Coriolis parameter at the southern boundary.

We evolve the model using a split timestepping method (Hallberg, 1997) with a baroclinic timestep of $\Delta t = 300$ s and a barotropic timestep of $\Delta t_{\text{BT}} = 30$ s. Isopycnal advection is computed using the energy conserving scheme of Sadourny (1975), while mass flux in the continuity equation is computed using a PPM finite volume method (Colella and Woodward, 1984; Lin et al., 1994).

The surface wind forcing and bathymetry are shown in Fig. 1. Surface forcing is an idealised zonal wind stress with a truncated sinusoidal profile across the central 80% of the channel, bounded from the south and north at latitudes $y_s = 0.1L_y$ and $y_n = 0.9L_y$, respectively. The wind stress is applied as an explicit acceleration of the top 20 m of the ocean, which is then redistributed across the exposed water columns as a reduced forcing. The bathymetry is a narrow Gaussian ridge across the channel of the form

$$H(\boldsymbol{x}) = H_0 e^{-(x/L)^2} \tag{1}$$

where $H_0 = 2500$ m and $L = 256$ km. The model contains no diapycnal mixing, ensuring that the mass of each layer is conserved. For the isopycnal flow, we use a fixed biharmonic viscosity of magnitude $A_4 = 10^{10}\ \text{m}^4\ \text{s}^{-1}$. A small quadratic bottom friction of the form

$$\mathcal{F} = C_d|\mathbf{u}|\mathbf{u} \tag{2}$$

is applied to bottom layers exposed to bathymetry, using a drag coefficient of $C_d = 3 \times 10^{-3}$.

Table 1
Initial stratification and associated baroclinic deformation radii λ_m. The reduced gravities g' are associated with the interfaces above each layer.

Layer	Depth (m)	g' (m s^{-1})
1	300	0.98
2	550	0.01
3	550	0.005
4	1300	0.005
5	1300	0.005

Mode	λ_m (km)
1	30.3
2	17.7
3	13.5
4	9.6

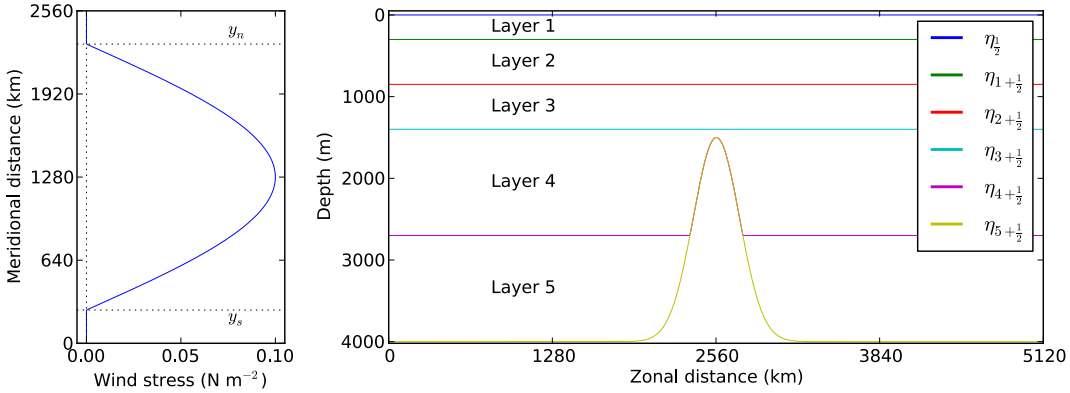

Fig. 1. Wind stress and bathymetry profile.

2.2. Momentum balance

Transfer of momentum within each isopycnal layer and across layers is determined using the momentum balance equation. For an isopycnal layer k bounded above and below by interfaces $\eta_{k-1/2}$ and $\eta_{k+1/2}$, respectively, the momentum balance can be expressed in terms of the pressures along each interface, so that the isopycnal momentum transport equation (derived in Appendix A) is

$$\frac{\partial}{\partial t}(h_k\boldsymbol{u}_k) + \nabla\cdot\left(h_k\boldsymbol{u}_k\boldsymbol{u}_k + \frac{1}{2}h_k\left(p_{k-\frac{1}{2}}+p_{k+\frac{1}{2}}\right)\boldsymbol{I}\right) + f\hat{\boldsymbol{z}}\times(h_k\boldsymbol{u}_k) = p_{k-\frac{1}{2}}\nabla\eta_{k-\frac{1}{2}} - p_{k+\frac{1}{2}}\nabla\eta_{k+\frac{1}{2}} + \tau_k \tag{3}$$

where τ_k denotes external forcing, such as surface wind stress or bottom friction, and $\boldsymbol{I}$ is the identity tensor. Momentum is transferred diapycnally by the form stress, $p\nabla\eta$. In this study we focus on the zonally averaged balance of zonal momentum density, $\overline{hu}|_k$, whose transport equation is

$$\frac{\partial}{\partial t}\overline{hu}|_k + \frac{\partial}{\partial y}\overline{(hu)v}|_k - f\overline{hv}|_k = \overline{p\eta_x}|_{k-\frac{1}{2}} - \overline{p\eta_x}|_{k+\frac{1}{2}} + \tau_k \tag{4}$$

where overbars denote zonally averaged quantities. This equation can be extended to the lower blocked layers if we interpret the regions of intersection with topography as if they are layers of zero thickness, with interfaces following the bathymetry.

2.3. Layer-integrated analysis

The equilibrium zonal transport is determined by the zonal momentum balance Eq. (4). The layerwise and total channel transport are, respectively,

$$T_k = \int_0^{L_y} h_k u_k\,dy, \quad T_{\text{sum}} = \sum_{k=1}^{N} T_k \tag{5}$$

Integration across the channel, assuming free-slip boundaries, determines the net momentum balance for each layer,

$$\frac{\partial T_k}{\partial t} = \int_0^{L_y} f\overline{hv}|_k\,dy + \int_0^{L_y}\overline{p\eta_x}|_{k-\frac{1}{2}}\,dy - \int_0^{L_y}\overline{p\eta_x}|_{k+\frac{1}{2}}\,dy + \int_0^{L_y}\tau_k\,dy \equiv C_k + S_{k-\frac{1}{2}} - S_{k+\frac{1}{2}} + F_k \tag{6}$$

where C_k is the net Coriolis force on layer k by meridional transport, $S_{k\pm1/2}$ is the interfacial form stress along interface $\eta_{k\pm1/2}$, and F_k is the external force applied to layer k by the surface wind stress. We note that $S_{N+1/2}$ is the topographic form stress along the bottom interface $\eta_{N+1/2}$ in an N-layered system.

The interfacial form stresses act as interior constraint forces between adjacent layers, and they cancel in the total force balance of the channel. That is,

$$\sum_{k=1}^{N}\left(S_{k-\frac{1}{2}} - S_{k+\frac{1}{2}}\right) = S_{\frac{1}{2}} - S_{N+\frac{1}{2}} \tag{7}$$

Additionally, there is no atmospheric pressure ($p_{1/2}=0$) in our simulations, and no corresponding surface form stress ($S_{1/2}=0$). The total force balance along the channel is

$$\frac{\partial T_{\text{sum}}}{\partial t} = C - S_{N+\frac{1}{2}} + F \tag{8}$$

where $C=\sum_{k=1}^{N}C_k$ is the net Coriolis force due to all meridional transport and $F=\sum_{k=1}^{N}F_k$ is the total forcing by surface winds. At equilibrium, the total zonal transport is constant and (from mass balance) the total meridional transport is zero, which implies that $C=0$. Hence, the equilibrium force balance is $F=S_{N+1/2}$; surface wind stress is balanced by bottom topographic form stress. For individual layers at equilibrium, the top layer satisfies $F=S_{1+1/2}$ (discounting any outcroppings), while the interior layer force balance is $S_{k-1/2}=S_{k+1/2}$, illustrating a perfect transfer of momentum from winds to topography through the interfacial form stress.

2.4. Filtering

Because our solutions contain substantial high-frequency variability, we apply filtering to the data to diagnose the dominant force balance during spinup. The model time series output has a sampling period of $T_s=5$ days, to which we apply fourth-order low-pass Butterworth filters of designated 3 dB cutoff frequencies $\omega_c = 2\pi T_c^{-1}$ (with equivalent normalised digital frequencies $\Omega_c = \arctan(\pi T_s/T_c)$) where T_c is the designated cutoff period. The value of T_c for the filtered results is noted in each figure. The choice of cutoff period ranges from six months to five years, in order to best highlight the trends during each stage of spinup. The filtered results have also been shifted by the zero-frequency group delay $\tau_g = -d\phi(\omega)/d\omega|_{\omega=0}$ where $\phi(\omega)$ is the spectral Butterworth filter phase shift. This restores the phase of any monotonic trends and low-frequency signals at the cost of phase shift errors in the high-frequency components near or above the cutoff frequency ω_c.

3. Results

An overview of the upper layer circulation profile during spinup is shown in Fig. 2. The general trend is from laminar Ekman transport (Fig. 2a) towards a turbulent final state of strong mesoscale eddies and jets (Fig. 2e) balanced around a mean state consisting of several zonal jets (Fig. 2f). We first demonstrate the layer-integrated force

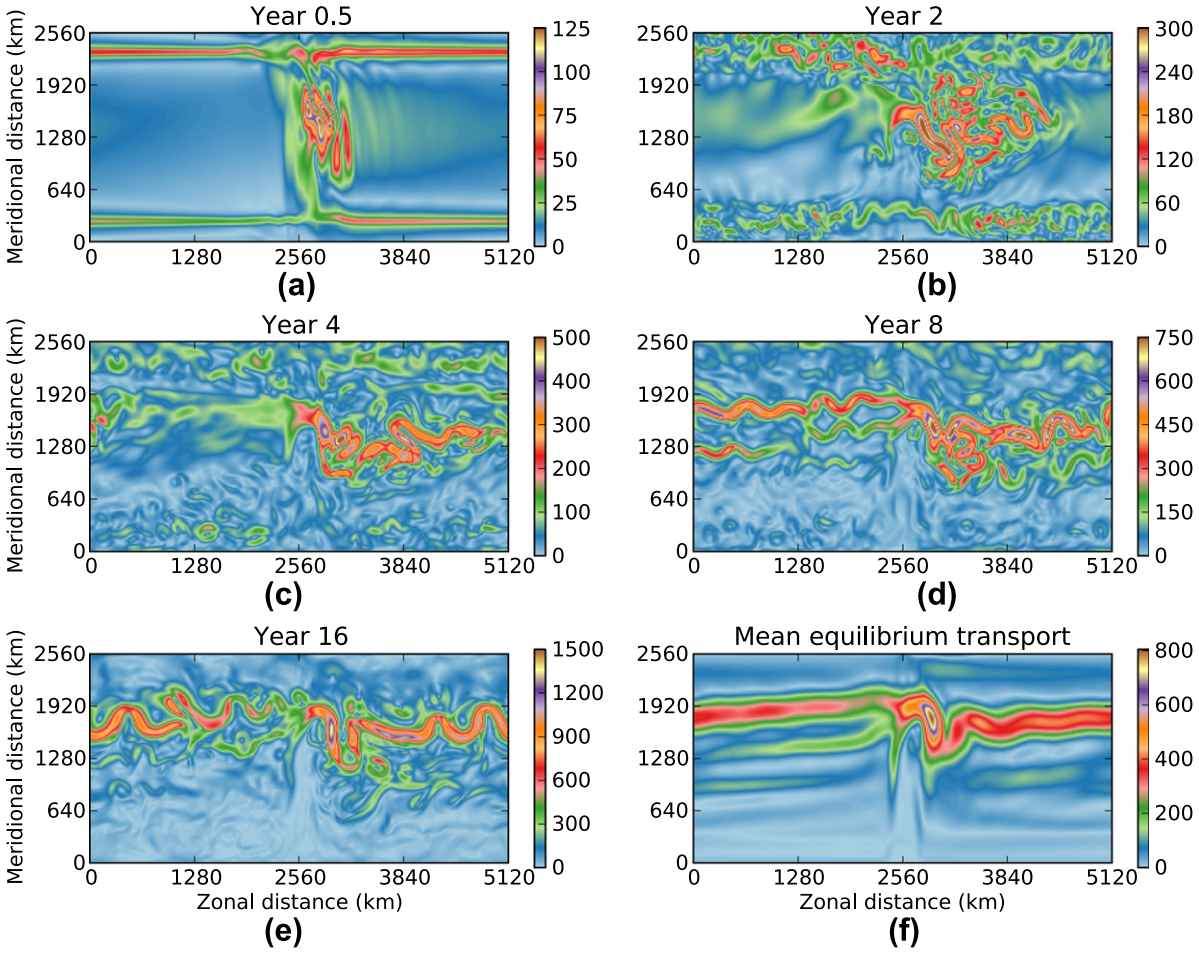

Fig. 2. The upper layer momentum magnitude $|h\mathbf{u}|$ ($m^2\,s^{-1}$) in the top two isopycnal layers during model spinup. Fig. 2a characterises the initial Ekman spinup. Fig. 2b–d illustrate the formation of the zonal jets during mesogenesis. Fig. 2e shows a typical circulation during form stress relaxation, and Fig. 2f shows the mean zonal transport at a form stress equilibrium.

balance and the transition from a Ekman layer to a form stress balance. This is followed by a comparison of our results to an idealised quasigeostrophic spinup of Anderson and Gill (1975). We end with a detailed analysis of the zonally averaged momentum balance for each layer.

3.1. Layer integrated balance

We first present the total force balance of the isopycnal layers during spinup. Figs. 3 and 4 show the initial and final spinup time series for the zonally averaged net zonal transport in each layer and the net interfacial form stress along each interface, as well as the net zonal Coriolis force produced by the meridional transport, as defined in Eqs. (5) and (6). Due to the emergence of an outcropping of the interface $\eta_{1+1/2}$, as well as the intense coupled variability between the blocked bottom layers, we combine the total Coriolis forces applied to the top two and bottom two layers and present them as single quantities, which allows us to illustrate the interior force balances and the transition to equilibrium as lucidly as possible. Low-pass filtering has also been applied to the longer time series of Fig. 4 in order to remove the high-frequency variability of the system during later times.

The time series reveal several major transitions in the evolution and equilibration of the wind-driven model current. We identify four major regimes during model spinup, which are based on the relationship between the net transport and the forces experienced by each layer. The different regimes, separated by dashed vertical lines, illustrate the general transition of the current from a balance maintained by Coriolis forces to one maintained by interfacial form stress.

The first regime, which we associate with the first year of model spinup, is established after an initial adjustment period of approximately three to six months. The system equilibrates to a state consisting of a weak zonal transport of approximately 2 Sv, as shown in Fig. 3a. Although the total transport appears small, the actual circulation consists of a broad eastward current opposed by narrow westward currents near the boundaries, which can be inferred from Fig. 2a. The net result of this flow is a near-cancellation of transport in the upper layers. For the channel as a whole, the surface wind forcing (denoted by horizontal dashed lines in the form stress and Coriolis force plots) is balanced by the topographic form stress $S_{5+1/2}$, shown in Fig. 3b, that develops approximately 25 days after initialisation. However, the force balance of each layer is sustained predominantly by Coriolis forces, shown in Fig. 3c, which emerge during this period. The top layer is in a typical Ekman layer balance, where eastward surface winds are balanced by westward Coriolis forces induced by a northward meridional transport. The bottom layers exhibit a similar balance, except that there is a southward transport whose eastward Coriolis forces are balanced by the westward topographic form stress along the bottom (with a partial contribution by $S_{4+1/2}$ along the topographic ridge). Any minor force imbalances between the winds, Coriolis forces, and topographic form stress are counterbalanced by a reduced interfacial form stress along the interior layers, but the transport within

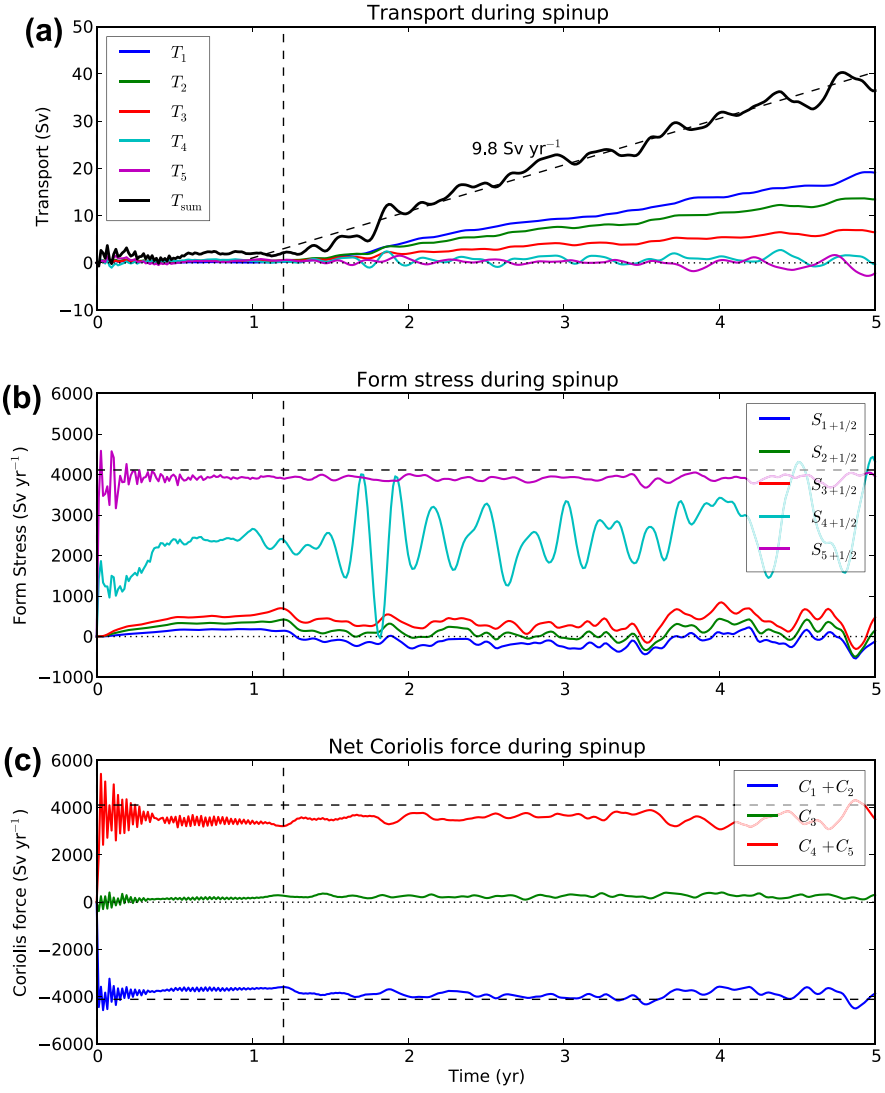

Fig. 3. Time series of the zonally averaged and latitudinally integrated (a) layer transport, (b) interfacial form stress, and (c) layer Coriolis force for the first five model years of channel spinup, as defined in Eqs. (5) and (6). The initial Ekman spinup regime is to the left of the vertical dashed line, and the mesogenesis regime is to the right. Surface wind stress is denoted by the horizontal dashed line in (b) and (c). The negative value of wind stress is also included in (c) for reference.

these layers is small and their contribution to the dominant force balance is negligible. Since the circulation is primarily characterised by Ekman transport, we refer to this regime as *Ekman spinup*. Aside from the initial 2 Sv transport, no acceleration of the total transport occurs during Ekman spinup, and this period lasts until approximately one year after initialisation.

The second regime is associated with the onset of zonal transport acceleration and the development of upper level jets. The transition is abrupt, after which the channel experiences a steady acceleration of approximately 10 Sv yr^{-1}, as shown in Figs. 3a and 4a. This period is characterised by greater variability and a slight reduction of interfacial form stress along the upper interior layers. However, the dominant force balance within the layers remains largely unchanged; surface winds remain balanced by Coriolis forces from a net northward transport in the top layer, while topographic form stress remains balanced by southward transport. The exception is a rising interfacial form stress $S_{4+1/2}$ along the top interface of the topographically blocked layer $\eta_{4+1/2}$, shown in Fig. 4b. This change is coincident with a decrease in southward transport and reduction of Coriolis forces on layer 5, as well as an increase in southward transport in layer 4 (not shown), even though the net effect on both layers is a negligible change in meridional transport and Coriolis forcing (Fig. 4c). But it is the first indication of changes to the meridional transport in the channel, and a transition from a state of Ekman layer balance to a balance consisting solely of interfacial form stress. We refer to this regime as *mesoscale genesis* or *mesogenesis* due to the emergence of mesoscale eddies and narrow zonal jets in the channel, as shown in Fig. 2b, which contribute to the interfacial form stress on the layers. Mesogenesis persists until about 7 model years after initialisation, after which the meridional transport ceases in the bottom layer and $S_{4+1/2}$ matches the topographic form stress $S_{5+1/2}$.

The third regime begins after the blocked bottom layer completes the transition from an Ekman layer to a form stress balance. After $S_{4+1/2}$ matches the topographic form stress $S_{5+1/2}$, the form stress along the upper layers begins to increase, emulating the same process of decreasing meridional transport and increasing interfacial form stress. This transition is also reflected in the upper layer zonal transport, which begins to asymptote towards an equilibrium value. An exception to this behaviour is the form stress $S_{1+1/2}$, which trends towards a lower value than the form stress along the other interfaces. This is due to the outcrop of interface $\eta_{1+1/2}$, which partially exposes layer 2 to the surface, where the role of form stress is effectively replaced by surface winds. Since the

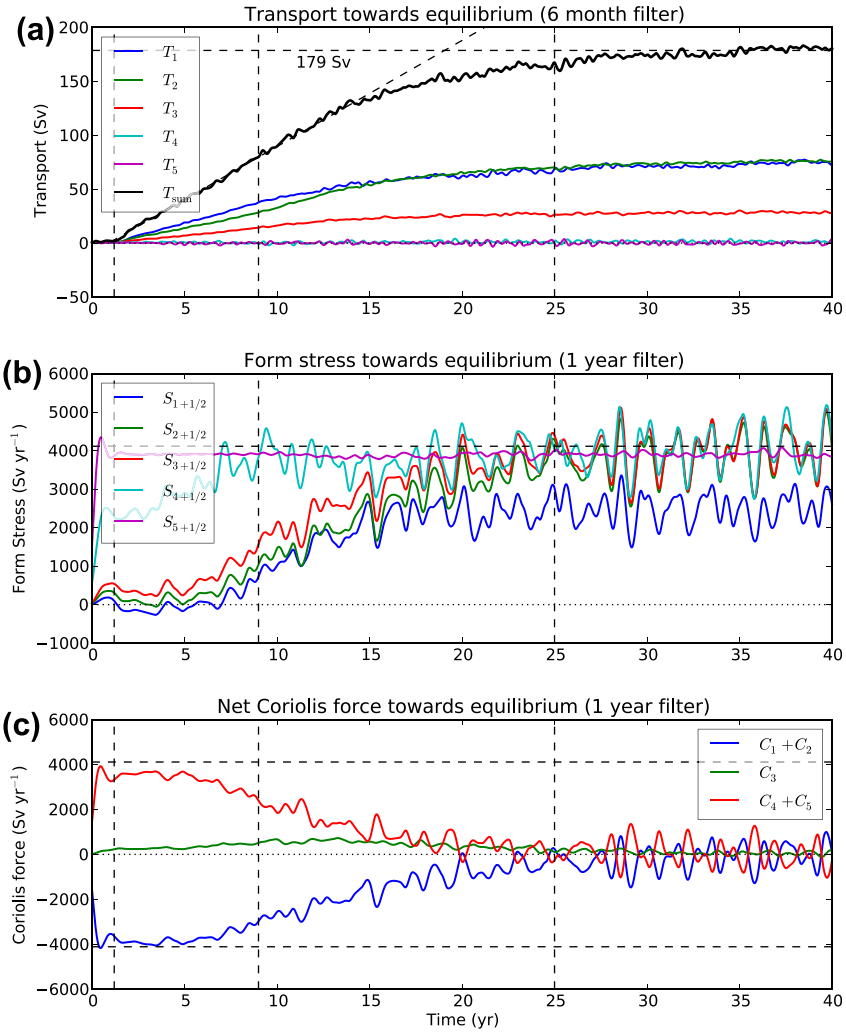

Fig. 4. Time series of the first 40 model years of spinup, as in Fig. 3. The four regimes discussed in the text are separated by the three vertical dashed lines.

form stress relaxes towards its equilibrium profile during this stage, which reduces the Ekman transport and equilibrates the zonal transport, we refer to this regime as *form stress relaxation*. Approximately 25 models years after spinup, the interfacial form stress of each layer matches the bottom form stress and there is no net Ekman transport.

The fourth regime describes the equilibrated current after each layer has shifted from an Ekman layer balance to a form stress balance, and we classify this regime as one of *form stress equilibrium*. The net zonal transport during this period is approximately 180 Sv. The mean zonal transport remains balanced after reaching this equilibrium with no noticeable drifts for the rest of the 100 year simulation.

Our numerical simulations confirm that the dominant force balance of the channel is between the surface wind stress F and the bottom topographic form stress $S_{5+1/2}$. However, $S_{5+1/2}$ develops within a few weeks after initialisation and remains relatively constant throughout channel spinup, providing little indication of the equilibrated state. Rather, equilibrium is associated with the cessation of Ekman transport within individual layers and with the development of interfacial form stress between the layers.

3.2. Rossby wave spinup

The timescale associated with the initial Ekman spinup is a direct consequence of the baroclinic instability growth rate, which has a relatively straightforward dependence on model parameters and the surface wind profile. For the purposes of this study, we simply note that there is an initial period of laminar spinup with negligible zonal transport during this time, after which there is an emergence of mesoscale structure. After this initial stage, the model experiences a nearly constant acceleration of transport. In this section, we argue that this acceleration can be interpreted as a consequence of wind-forced Rossby waves. The analysis of Anderson and Gill (1975) (herein AG75) illustrates how Rossby wave propagation creates an equilibrium current in a stratified ocean basin. To demonstrate this process, they consider an ocean that is bounded by rigid meridional shelves at $x = \pm L$ while remaining periodic in the meridional direction, y. The ocean is forced from a state of rest by a zonal surface wind stress of the form $\tau = \tau_0 \sin ly$. By assuming linearised dynamics and decomposing the flow into vertical and meridional modes, they show that the amplitude of the zonal velocity mode u satisfies a Rossby wave equation of the form

$$(u_{xx} - \mu^2 u)_t + \beta u_x = -l^2 \left(\frac{\tau_0}{H_{\text{mix}}} \right) \tag{9}$$

along with the boundary conditions $u = 0$ at $x = \pm L$, where

$$\mu^2 = \left(\frac{f}{c} \right)^2 + l^2 \tag{10}$$

and c and H_{mix} are the gravity wave speed and projected mixed layer depth, respectively, for the corresponding vertical mode. If

the meridional lengthscale l^{-1} of the wind is large and we focus our attention on the baroclinic modes, such as in our model simulations where $l^{-1} \sim 1000$ km and $c/f \sim 10$ km, then $\mu \approx f/c$ and μ^{-1} characterises the deformation radius for the baroclinic modes. AG75 constructs an approximate spinup solution based on boundary layer theory applied along the western shelf, motivated by the generation of wind-forced Rossby waves. The faster westward propagation of large-scale Rossby waves from the eastern shelf establishes the interior Sverdrup balance, while the slower eastward propagation of the small-scale waves from the western shelf develops into a boundary current. For our purposes, we focus on the formation of the interior flow, where zonal variation by the large-scale Rossby waves can be assumed to be negligible. Under this idealisation, the Eq. (9) for u has the approximate form

$$-\mu^2 u_t = -l^2\left(\frac{\tau_0}{H_{\text{mix}}}\right) \tag{11}$$

which has the solution

$$u = \left(\frac{l^2\tau_0}{\mu^2 H_{\text{mix}}}\right)t \tag{12}$$

describing an approximate resonant forcing of the large-scale waves during the early stages of spinup. This solution is expected to persist for a time interval $T_{\text{eq}} \sim \mu^2 L/\beta$ after which the westward Rossby waves have crossed the basin. After T_{eq}, reflection and dispersion begin to disrupt this resonance and the interior readjusts towards a Sverdrup balance.

Our model simulations differ from these idealised conditions in several respects. Our channel is zonally re-entrant and lacks rigid meridional shelves, and it is not periodic in the meridional direction. Nonlinear interactions by the mesoscale are also prevalent in our simulations. But there are enough similarities to the idealised system to justify an exploration of the Rossby wave spinup as described in AG75. For example, our topographic ridge is steep enough that it blocks the barotropic PV contours, which can restrict the zonal transport in the same manner as a rigid boundary. The assumption of meridional periodicity is primarily of mathematical convenience, and is not required to reproduce the qualitative results of AG75. There is also evidence of topographically trapped Rossby waves during spinup, evidence of which can be observed in Fig. 2a, and the linear increase of zonal transport during mesogenesis resembles the prediction of (12) by AG75. These facts motivate us to interpret our periodic zonal channel as a basin wedged between two sharp topographic ridges, and to investigate the role of trapped Rossby waves on the baroclinic modes of the channel.

We diagnose the role of Rossby waves in spinup by comparing the early linear growth rate of zonal transport of several simulations with different parameters. First, we note that an increase in the amplitude of a sinusoidal mode of u does not necessarily correspond to an increase of zonal transport. In AG75, the zonal flow is periodic along the meridians and a rising amplitude will increase both eastward and westward flow. To produce the transports observed in Figs. 3 and 4, some additional localised forcing would be required to preferentially suppress westward transport while leaving eastward transport intact. In Section 3.3, we attribute this forcing to interfacial form stress from the mesoscale flow. Second, the results of AG75 describe the response of a single baroclinic mode, but we do not discuss the structure of such modes, nor the degree to which the wind stress, form stress, or zonal transport projects onto any individual mode. Instead, we modify parameters which impact all baroclinic modes equally, and interpret our results as the aggregate baroclinic response.

In order to apply Eq. (12) to our results, we assume that the net transport T_{sum} scales with u and that T_{sum} reflects the cumulative impact of all baroclinic modes. We propose that T_{sum} satisfies an equation of the form

$$T_{\text{sum}} = \left(\frac{\tau\tilde{g}}{\tilde{f}^2}\right)Kt \tag{13}$$

during the early stages of spinup. This equation is constructed by first noting that $\mu^2 \approx f^2/c^2 = f^2/(g'H)$ for each baroclinic mode with an equivalent acceleration g' and depth H. If we restrict ourselves to parameters that rescale all baroclinic modes in equal proportion, then the parameter $\tilde{g}$ acts as a measure of the baroclinic accelerations. The constant K depends on the vertical mode projections and any unconsidered parameters, such as l, H, and H_{mix}. We can then relate the transports of different simulations by the equation

$$\frac{\left(\tilde{f}/\tilde{f}_c\right)^2}{(\tilde{g}/\tilde{g}_c)(\tau/\tau_c)}T_{\text{sum}} = T_{\text{sum},c} \tag{14}$$

where the subscript c denotes the parameters from the control experiment in Section 3.1. If the rescaled transport time series on the left hand side of Eq. (14) match the control experiment transport, then the experiments are in agreement with the theory of AG75, and Rossby waves are responsible for the early spinup of the channel.

We apply Eq. (14) to experiments where we vary the wind stress τ, buoyant acceleration $\tilde{g}$, and Coriolis parameter $\tilde{f}$. The wind stress τ is defined as the maximum of the wind stress profile, denoted by τ_0 in Section 2.1. The parameter $\tilde{g}$ represents a cumulative measure of the interfacial accelerations g_j. A change in $\tilde{g}$ corresponds to a rescaling of g_j across all interior layers, while leaving the barotropic acceleration unchanged. For example, a doubling of $\tilde{g}$ denotes a doubling of the stratification at all levels. The Coriolis parameter $\tilde{f}$ is measured relative to its value in the centre of the channel, so that $\tilde{f} = f_0 + \beta L_y/2$ where f_0 is the value of f on the southern boundary. As a result, variations in β that leave f_0 unchanged will still result in changes to $\tilde{f}$.

Fig. 5 illustrates the change in transport during spinup as we vary τ, $\tilde{g}$, f_0 and β. During the early stages of spinup, nearly all of the experiments exhibit a transport acceleration that is consistent with Eq. (14). Fig. 5a, the rescaled transport versus τ, follows this trend over the first five model years, indicating that the early transport acceleration is proportional to τ. The figure also demonstrates that the equilibrium transport is not proportional to τ; instead, the equilibrium transport trends towards a value that is independent of τ (or a rescaled transport proportional to τ^{-1}) which is consistent with propositions of eddy-saturated transport. Fig. 5b shows that the rescaled transport is nearly independent of $\tilde{g}$, indicating that both the transport acceleration and equilibrium transport are proportional to $\tilde{g}$. Fig. 5c, which shows the rescaled transport versus f_0, shows the most noticeable discrepancies from Eq. (14). Unlike the other model simulations, these experiments show a delayed transition to mesogenesis that is roughly proportional to f, but whose subsequent acceleration is otherwise consistent with Eq. (14). The transport for the case $f_0 = \frac{1}{2}f_{0,c}$ undergoes an abrupt acceleration after five model years, which may be a consequence of the presence of unblocked barotropic PV contours. Fig. 5d shows that transport acceleration is largely independent of β, although the equilibrium transport increases monotonically with β. The case $\beta = 2\beta_c$ undergoes an abrupt acceleration after 10 model years in a manner similar to the case $f_0 = \frac{1}{2}f_{0,c}$ and shares the property of unblocked barotropic PV contours. The other exceptional case is $\beta = 0$, which shows very little zonal transport and is possibly a consequence of the absence of Rossby wave propagation.

These results demonstrate that early model spinup resembles the Rossby wave spinup of AG75 in several respects and suggest

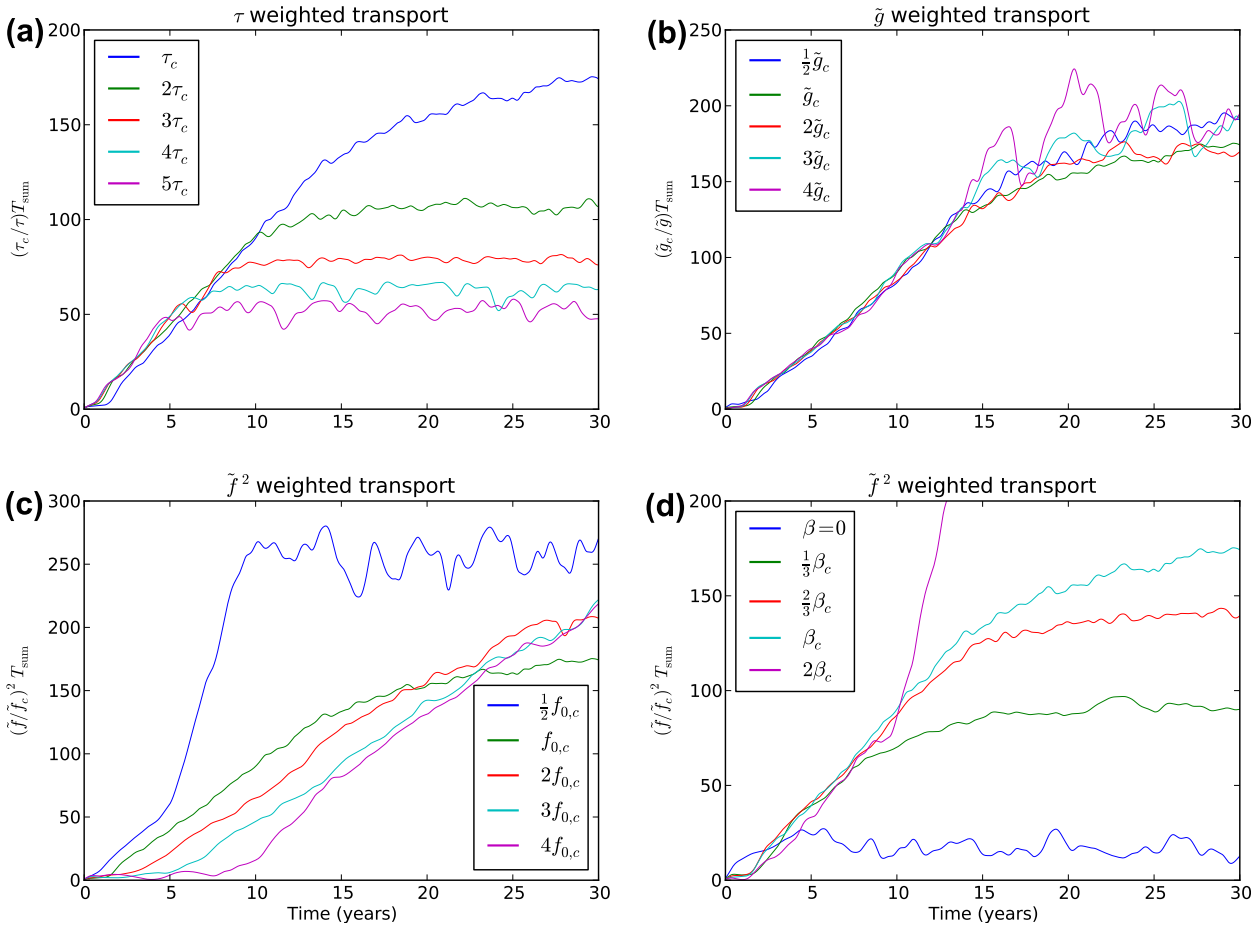

Fig. 5. The rescaled transport, as defined in (14), versus maximum wind stress (a), background stratification (b), coriolis parameter (c), and background vorticity gradient (d) over the first 30 model years of spinup (1 year filtering).

that Rossby waves are essential to the establishment of zonal transport in a re-entrant channel. Extension of the AG75 theory to the equilibrium state is complicated by the presence of a very strong background flow, where northward Ekman transport produces a deepening of isopycnals that modify the background PV gradient, which is further modified by turbulent stirring from baroclinic instability. In the next section, we demonstrate that interfacial form stress emerges as an alternative to a Sverdrup balance established by Rossby waves.

3.3. Zonal momentum balance

Section 3.1 identified four major regimes of spinup that characterised the transition of the channel circulation from Ekman spinup to form stress equilibrium, and Section 3.2 argued that the early spinup is a reflection of Rossby wave amplification. For this argument to be valid, there must exist some asymmetric response along westward jets, so that mode amplification results in an increase in the eastward flow and the zonal transport. In this section, we argue that interfacial form stress produces this asymmetric response through mesoscale eddies. For each flow regime, we focus on the zonally averaged momentum balance and present profiles of transport, form stress, Coriolis force, and eddy momentum flux. In order to reduce internal variability and to eliminate any data artefacts generated by surface outcropping, we combine the top two and bottom two layers as if they were single macroscopic isopycnal layers, and interpret the channel as a three-layer system.

3.3.1. Ekman spinup

A typical zonal transport profile during Ekman spinup is shown in Fig. 6a and consists of a broad eastward flow in the centre of the channel that is flanked to the north and south by concentrated westward jets. The zonally averaged force profiles corroborate the discussion in Section 3.1. For the most part, the surface wind stress is balanced by the bottom topographic form stress $\overline{p\eta_x}|_{5+1/2}$ at every latitude, as shown in Fig. 6b. Small amounts of interfacial form stress develop along the upper interior layers, but their magnitudes are small in comparison to the topographic form stress and can be regarded as a secondary influence. Individual layers are instead balanced by the Coriolis forces from steady meridional currents, shown in Fig. 6c. The surface winds are balanced by a northward meridional transport in the upper layers, and the topographic form stress is balanced by a southward meridional transport.

From these profiles, we can reconstruct the evolution of the channel circulation over the first year. The simulation begins at rest with flat isopycnals, and the sinusoidal wind stress profile τ is applied to the top layer after initialisation. This immediately excites high-frequency barotropic and baroclinic gravity waves throughout the channel, which produce the rapid oscillations observed in Fig. 3c. After approximately 25 days of geostrophic adjustment, the surface currents begin to organise themselves into an Ekman layer balance, whereby the zonal surface wind stress induces a steady northward meridional transport. This meridional Ekman flow transfers mass from y_s to y_n, which leads to a meridional tilt of the upper isopycnal interface and an eastward geostrophic current, as observed in the transport profile. Since there

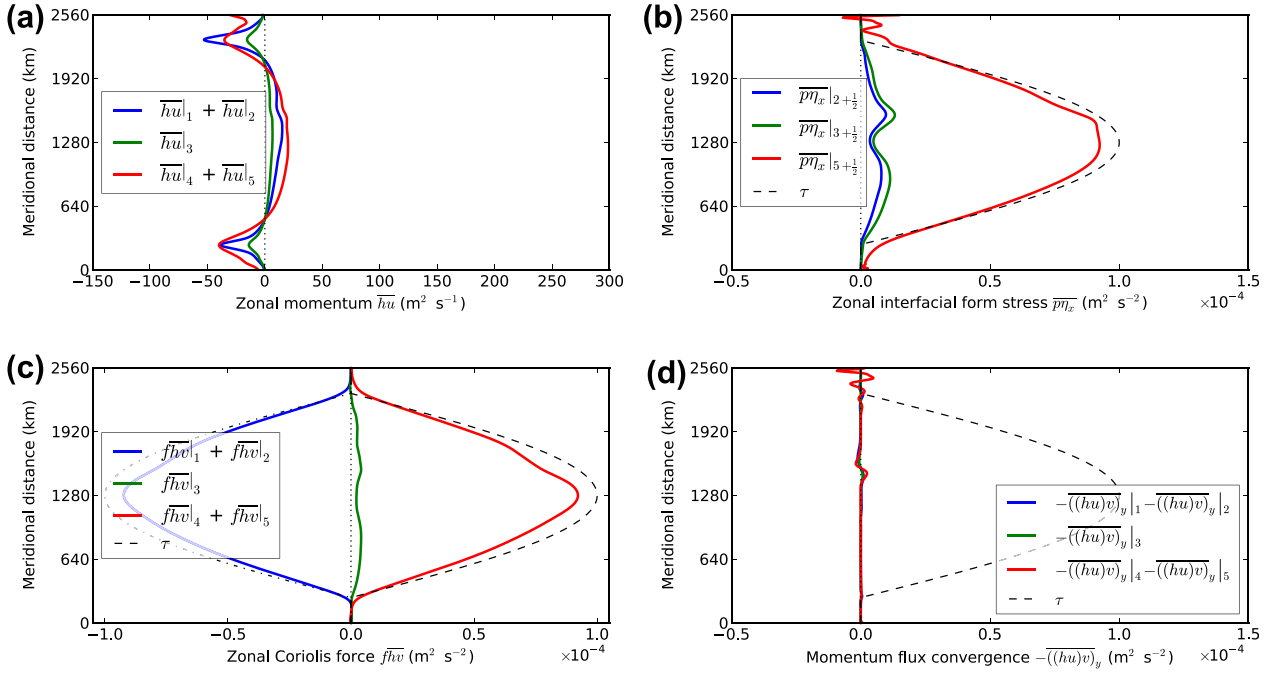

Fig. 6. Zonally averaged profiles of the (a) zonal transport per unit length, (b) form stress between isopycnal layers, (c) coriolis force induced by meridional transport, and (d) meridional flux convergence of zonal momentum. Profiles are shown during Ekman spinup (6 months after spinup, unfiltered).

is no wind stress or Ekman transport beyond y_s and y_n, the isopycnals remain flat outside of these latitudes. This creates a deficit and surplus of mass at y_s and y_n, respectively, which creates discontinuous isopycnal slopes at these latitudes, smoothed out by the small-scale dissipation of the model, which produces the narrow westward geostrophic jets observed at these latitudes. This trend is mirrored in the bottom layers, where a northward upper layer current induces a southward lower layer current, which produces eastward Coriolis forces that are balanced by the topographic form stress.

The interior layers remain relatively inert and the circulation remains predominantly laminar and noninertial during Ekman spinup, as indicated by the close agreement between the wind stress and force profiles as well as the absence of any substantial eddy momentum flux (shown in Fig. 6d). The baroclinic Rossby wave spinup remains unobservable in the zonally averaged profiles. But the perpetual increase of isopycnal slope across the channel and the accumulation of mass from y_s to y_n cannot be a sustainable circulation, and it is eventually disrupted by the emergence of baroclinic instabilities along the narrow westward jets.

3.3.2. Mesogenesis

During Ekman spinup, the flow is predominantly zonally invariant and the interfacial form stress remains a secondary consideration. But after approximately one year, the isopycnal slopes near y_s and y_n become sufficiently steep to induce baroclinic instability along the westward geostrophic jets, as indicated by the bands of turbulent eddies near y_s and y_n in Fig. 2b. The onset of baroclinic instability discourages additional isopycnal tilt near these latitudes, which constrains the transport of the upper level westward jets (Straub, 1993). The eastward jet in the centre of the channel retains most of its laminar structure, despite the emergence of a turbulent wake downstream of the topography, and the northward Ekman transport persists across the channel interior. Mass continues to be shifted northward and the isopycnal slope continues to rise, which accelerates the central eastward transport and can be interpreted as a consequence of the near-resonant forcing of the baroclinic Rossby wave modes. A representative transport profile during this period is shown in Fig. 7a, which shows both the intensified westward jets and the strengthened eastward current.

The mesoscale eddies generated by the baroclinically unstable westward jets introduce substantial zonal variability near these latitudes, which leads to increased upper level interfacial form stress in opposition to the westward jets, demonstrated by the negative anomalies of $\overline{p\eta_x}$ at y_s and y_n in Fig. 7b. Interfacial form stress also develops along the central eastward jet due the formation of eddies in the downstream wake of the topographic ridge. The form stresses in each direction tend to balance each other, so the integrated transport of the upper ocean remains in an Ekman layer balance. But the turbulent circulation introduces local imbalances between the surface winds and Coriolis forces, and Fig. 7c shows that the channel is no longer in a pure Ekman layer balance at every latitude, characterised by the reduced meridional transport across the interior and the emergence of transport beyond y_s and y_n. The meridional transport beyond the region of wind forcing allows mass to accumulate from the southern to northern boundaries in such a way that the interface heights can rise and lower along the northern and southern boundaries, respectively. This produces a net isopycnal slope across the upper layers, which suppresses the westward jets and triggers the net eastward transport acceleration observed in Figs. 3a and 4a. There is also an emergence of turbulent eddy flux of zonal momentum, shown in Fig. 7d, but it remains a secondary consideration in the force balance of the channel.

During this period of emergent upper layer interfacial form stress, there is a subtle trend of rising form stress along the blocked interface $\eta_{4+1/2}$, seen in Fig. 4b. As long as the upper layers remain balanced by Coriolis forces, the net zonal transport acceleration remains approximately constant. This persists until the form stress along the blocked interface matches the topographic form stress.

3.3.3. Form stress relaxation

The zonally averaged flow begins to trend towards a more persistent equilibrium state after the blocked lower layers equilibrate

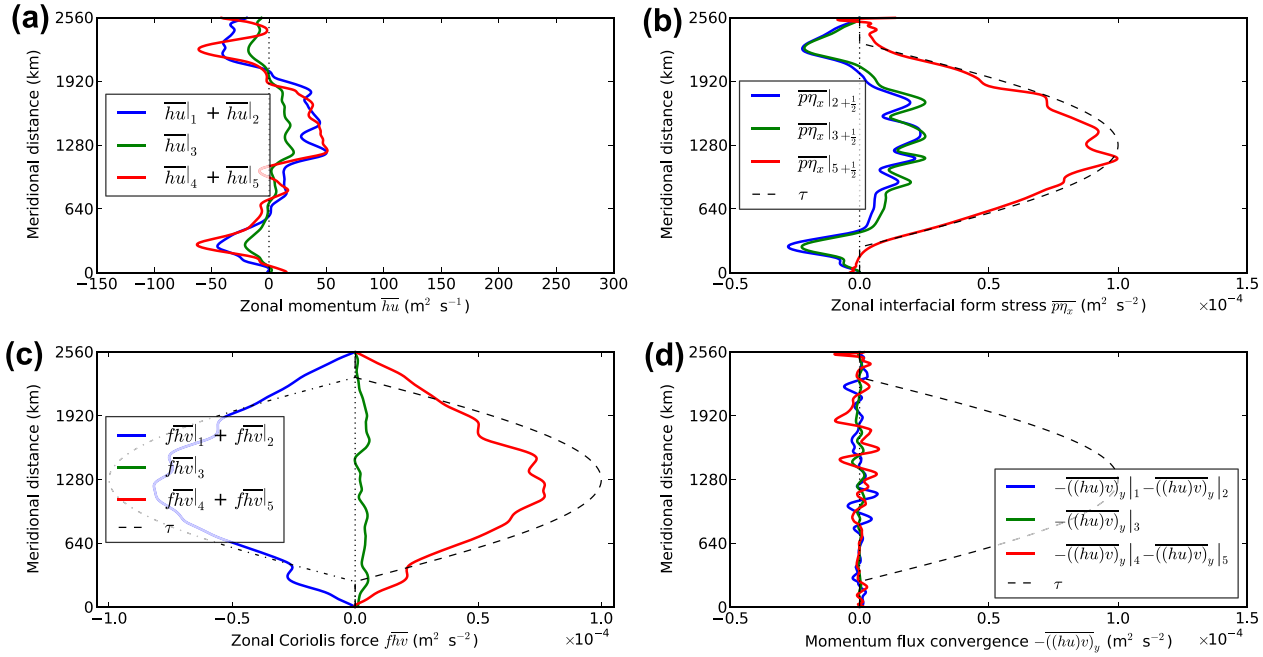

Fig. 7. As in Fig. 6, during mesogenesis (2 model years after spinup, using a 6 month low-pass filter).

and shift from an Ekman layer balance to a form stress balance. Eight model years after initialisation, the upper layer transport is concentrated into visibly coherent zonal jets, as seen in Figs. 2d and 8a. The upper layer form stress in the centre of the channel also begins to increase at this stage, reflecting the increase in mesoscale eddy activity throughout the channel. This trend is illustrated in Fig. 8b, which shows a prominent peak of interfacial form stress across the centre of the channel. The form stress from the westward jets has started to recede, leading to the net increase in form stress observed in Fig. 4b. There is a decrease in meridional transport as the channel geostrophically readjusts to the higher zonal form stress, producing the reduced Coriolis force profiles in Fig. 8c. There is also an increase of meridional advection of zonal momentum within the eastward transport, shown in Fig. 8d, which contributes to the formation of narrow eastward jets.

These trends are exacerbated in Fig. 9, which shows the mean force profiles sixteen model years after initialisation. The flow is now dominated by mesoscale eddies and meandering jets, such as observed in Fig. 2e, and these conditions characterise the flow for the rest of the simulation. By this stage, the northern jet in the transport profile of Fig. 9a has intensified and now dominates the channel. Additional jets have also emerged as the system approaches a state of dynamic equilibrium. Interfacial form stress has increased at all levels, and the profiles in Fig. 9b nearly match

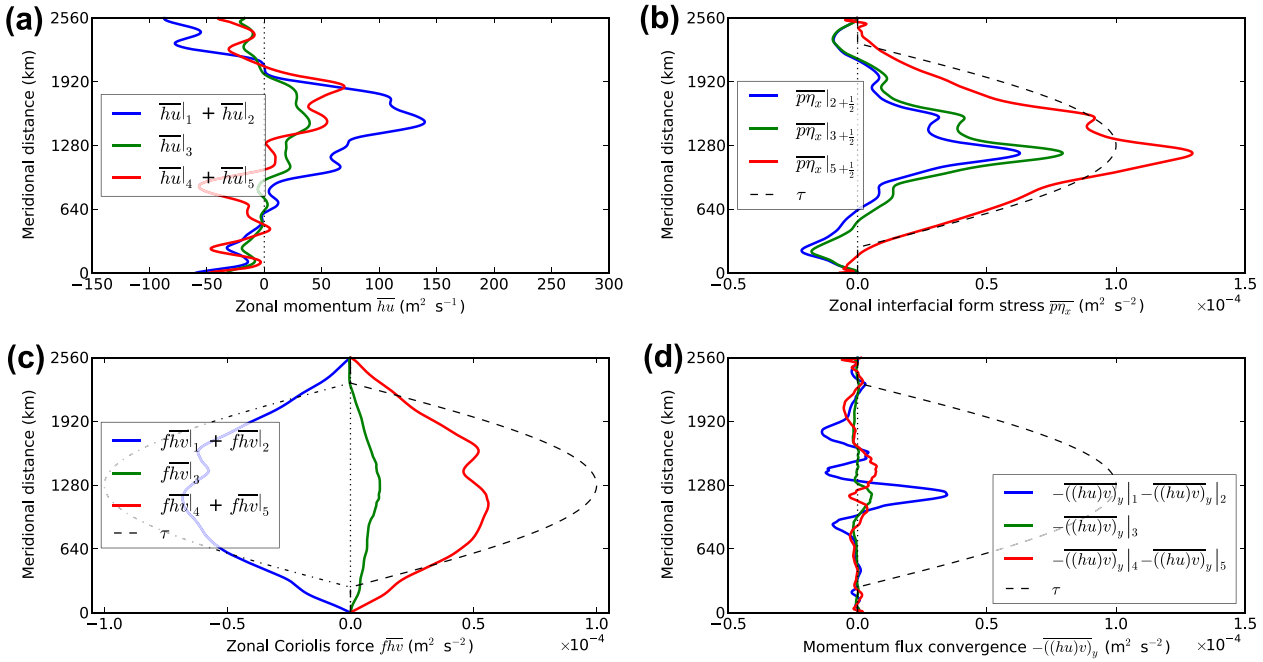

Fig. 8. As in Fig. 6, during the transition from mesogenesis to form stress relaxation (8 model years after spinup, using a 2 year low-pass filter).

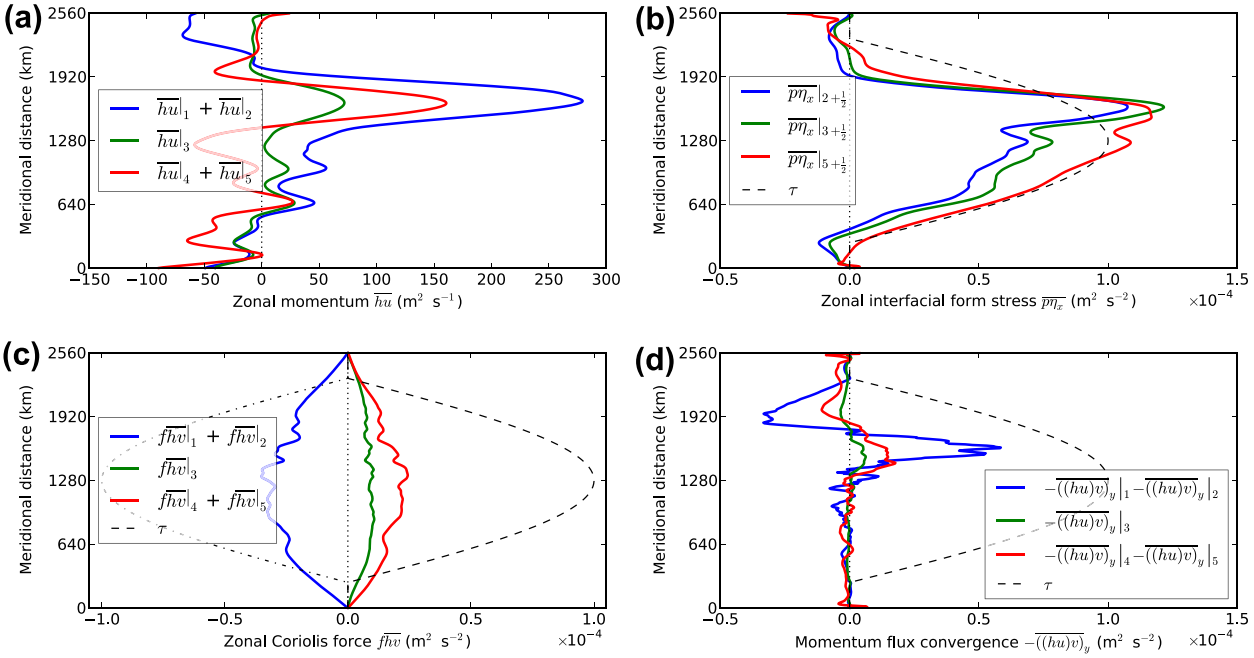

Fig. 9. As in Fig. 6, during form stress relaxation (16 model years after spinup, using a 5 year low-pass filter).

the topographic form stress at all latitudes. Meridional transport has also greatly diminished across the channel, as seen in Fig. 9c, as form stress sustains the applied wind stress. The reduction in meridional transport also reduces the rate of isopycnal tilt and slows the transport towards equilibrium, as observed in Fig. 4a. The increase in transport is also associated with a rise in meridional eddy transport of zonal momentum, which contribute to the concentration of momentum into narrow zonal jets.

The emergence of interfacial form stress and reduction of meridional transport is a symptom of a reduced background PV gradient and Rossby wave activity, which relaxes the net zonal transport of the channel and pushes the system towards a state of dynamic equilibrium. This process continues until the form stress matches the applied wind stress at all levels, and the transport equilibrates to a mean state.

3.3.4. Form stress equilibrium

After approximately 30 model years, the channel reaches a state of form stress equilibrium. At any particular moment, the equilibrium flow qualitatively resembles Fig. 2e, with strongly time-dependent features such as meandering jets and energetic mesoscale eddies. But amidst this variability is a persistent mean flow along the channel, shown in Fig. 2f, which consists of a strong northern jet and several progressively weaker jets to the south.

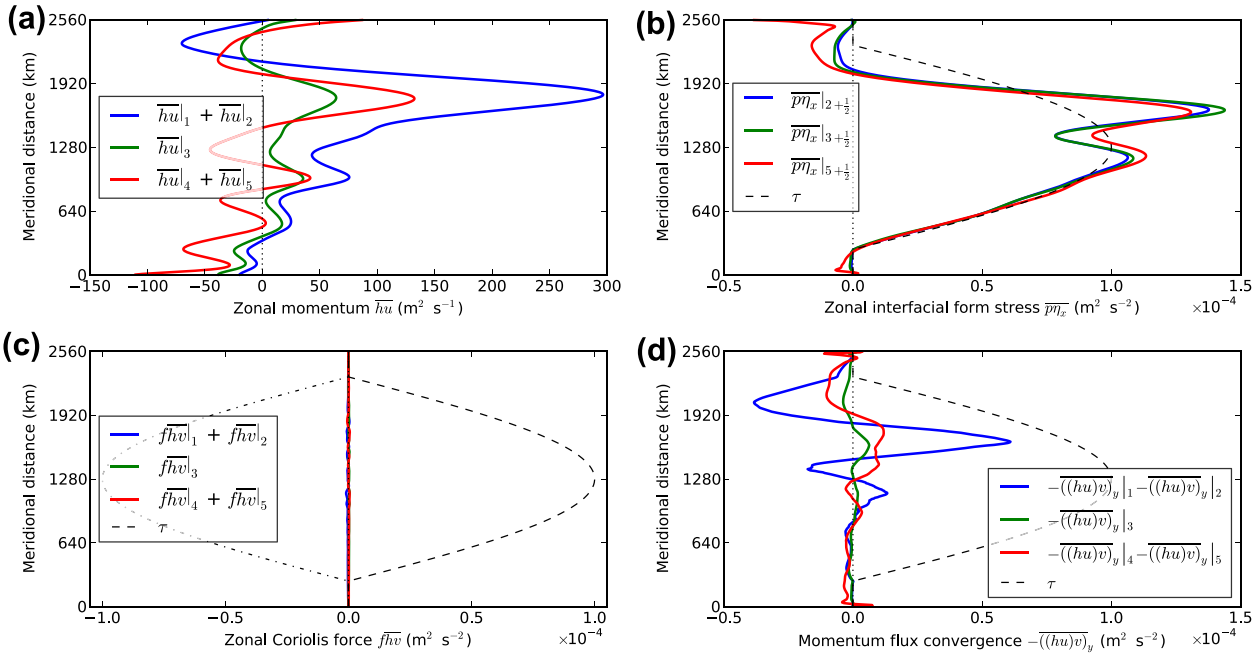

Fig. 10. As in Fig. 6, for the mean state during form stress equilibrium (70 year average).

Fig. 10a shows three dominant zonal jets across the channel, as well as several secondary jets near the boundaries. The mean state does not necessarily reflect the transport at any particular moment, since the jets meander over distances exceeding 100 km, and their structure changes considerably as they shed and absorb large mesoscale eddies. Despite this variability, the mean force balance remains robust. Each layer is balanced by the form stress shown in Fig. 10b. There is little difference between the form stress of adjacent layers, so that the upper form stress on interior layers is balanced by the form stress from below at every latitude. The only major discrepancy is between the surface winds and upper interfacial form stress $S_{2+1/2}$, which is not sustained by the Coriolis forces of the meridional transport, which has receded completely (Fig. 10c), but by eddy fluxes of zonal momentum from regions of low to high regions of form stress (Fig. 10d). The elevated regions of form stress are also in the vicinity of the zonal jets, which are themselves maintained by the eddy momentum flux.

The final equilibrium state persists for the remaining 70 model years of the 100 year simulation, and is maintained by a combination of interfacial form stress and eddy momentum fluxes. While the dominant transfer of momentum is from surface winds to bottom topographic form stress, the momentum advection profiles indicate that there is a secondary exchange of momentum between different latitudes produced by the mesoscale circulation.

4. Discussion

From the results shown here, we can summarise the model spinup and momentum balance as follows. After a brief period of geostrophic adjustment, Ekman layers develop in the top and bottom layers driven by wind stress and topographic form stress, respectively. Meanwhile, the baroclinic modes also become excited by the wind forcing and develop through resonant forcing of baroclinic Rossby waves. As the Ekman transport increases the isopycnal tilt, the upper layers become baroclinically unstable and mesoscale eddies develop along the narrow westward jets. Through these eddies, there is an increase of interfacial form stress and a transfer of momentum from the baroclinic to barotropic modes which halts the westward flow while permitting the eastward flow to continue accelerating, producing the observed zonal transport during mesogenesis. This transfer of zonal momentum from baroclinic Rossby waves to barotropic transport continues until the mesoscale activity of the barotropic flow becomes sufficiently turbulent and the interfacial form stresses balance the wind stress across all vertical modes. After this stage, the flow remains in a dynamic equilibrium supported by mesoscale eddies.

Unlike previous quasigeostrophic studies, geostrophic adjustment is not an imposed constraint in our simulations but it remains the means through which equilibrium is established. The initial imbalance of the surface winds is resolved by the emergence of a northward Ekman transport in the upper layers after a period of geostrophic adjustment. The adjustment process also preserves mass balance by inducing the opposing southward transport in the bottom layers. Geostrophic adjustment resolves the Coriolis force imbalance of the bottom southward transport by inducing a pressure field that generates an opposing topographic form stress. The result of this process is an indirect transfer of momentum from the surface to the bottom, demonstrating that interfacial form stress is not the only means of diapycnal momentum transfer from surface winds to bottom bathymetry. Topographic form stress must always exist to prevent mass transport through the bathymetry, and geostrophic adjustment will accomplish this momentum transfer in the absence of interfacial form stress.

Geostrophic adjustment preserves the force balance of the model through subsequent stages of evolution, but plays a progressively smaller role as the zonal transport increases and the interfacial form stress becomes more prevalent. Ekman transport increases the isopycnal slope through meridional mass displacement, which in turn increases the geostrophic zonal transport and the diapycnal shear. These conditions make the current more baroclinically unstable, which amplifies the rate of energy transfer to small scales and leads to the formation of mesoscale eddies. These eddies create zonal disturbances of the interfaces within the isopycnal layers and subject the layers to increased levels of interfacial form stress as the current struggles to flow past them. Since the surface currents tend to flow in the direction of the wind stress, and since the form stress tends to act in the opposite direction of the currents, the net force imbalance on the layers is reduced over time. The Ekman transport required to balance the layers therefore tends to decrease as the system generates more mesoscale eddies. Eventually, the form stress will match the wind stress and there will be no Ekman transport. At this point, the isopycnal slope will stabilize and the circulation will approach a state that supports the balancing interfacial form stress. This scenario does not require a separate southward mass transport $\overline{hv}$ to balance the opposing northward Ekman transport. Rather, the form stress from the eddies oppose the surface wind stress and reduce the actual northward Ekman transport that is required to maintain geostrophic balance.

The relevance of our results to the ACC depends primarily on the sensitivity of the flow to the boundary conditions along the northern and southern boundaries. In our model, there can be no meridional transport at equilibrium, due to the presence of rigid zonal boundaries and the absence of any diapycnal processes. Equilibrium is defined as the circulation which produces no Ekman transport, which corresponds to a circulation whose form stress matches the surface wind stress along every interface. Since we are effectively prescribing the equilibrium meridional transport in each layer to be zero, the major question is whether our results reflect the conditions of the ACC. Because the Southern Ocean has an open northern boundary and supports diapycnal exchange, it is capable of supporting a nonzero meridional transport at equilibrium, defined either by the details of diapycnal transport, surface wind and buoyancy forcing, or by processes outside of the Southern Ocean.

If, for the sake of argument, we assume that the overturning is imposed externally, then the equilibrium circulation should behave similar to the results presented here, except that the system would equilibrate to a state with a reduced interfacial form stress and a nonzero Ekman transport. A Southern Ocean overturning transport of 20 Sv (Lumpkin and Speer, 2007) would subject the layers to a mean Coriolis stress $f\overline{hv}$ of approximately $10^{-4}\,\mathrm{m^2\,s^{-2}}$, which is comparable to the wind stress estimates based on observations, and suggests that there would be a mean imbalance of wind stress and interfacial form stress. In this case, we would expect that the presence of overturning would reduce the hypothetical wind-driven channel transport from any conceptual model. A more likely scenario is that the overturning and diapycnal exchange would have an impact on the background stratification and the isopycnal slopes, which would be reflected in the zonal transport. This could introduce further feedbacks into the system, in which case our results would only represent a single component of a much larger problem and the eventual equilibrium would become more difficult to forecast.

Regardless of the impact of the overturning, it is clear that the zonal circulation in the present model qualitatively resembles the strong frontal jets and mesoscale eddies observed in the Southern Ocean, and that such currents must contribute a substantial amount of interfacial form stress to the interior of the Southern Ocean. Transport cannot be determined solely by the rate of overturning, nor does the onset of baroclinic instability and emergence

of interfacial form stress from mesoscale eddies define the equilibrium state. Instead, equilibrium is determined by the interfacial form stress which shuts off the Ekman transport, or reduces it to a sustainable value. In each layer, we can state with reasonable confidence that the meridional transport is a diagnostic quantity; that is,

$$f\overline{hv}|_k \approx -\tau_k - \overline{p\eta_x}|_{k-\frac{1}{2}} + \overline{p\eta_x}|_{k+\frac{1}{2}} + \frac{\partial}{\partial y}\overline{(hu)v}|_k. \tag{15}$$

However, a robust model for the equilibrium zonal transport in a wind-driven model will require a more precise model for the zonal circulation required to produce the necessary form stress response. Baroclinic instability is the most likely source of mesoscale eddies and interfacial form stress, but it does not necessarily characterise the eventual equilibrium distribution of mesoscale energy. Our results do not resolve these issues, but they assert that any substantive theory of wind-driven zonal transport must either incorporate or parameterise the relationship between Ekman transport and form stress from mesoscale eddies in the Southern Ocean.

5. Conclusions

We have demonstrated that a zonal transport is achievable in a wind-driven isopycnal channel model with obstructive bathymetry, and that the equilibrium is regulated by the interfacial form stress produced by mesoscale eddies. Large-scale forces such as topographic form stress and Ekman transport maintain the force balance during the early stages of spinup, but play a secondary role in equilibration of the channel flow. Rather, it is the development of mesoscale jets and eddies throughout the channel and their contribution to the interfacial form stress that defines the equilibrium state. Meridional transports act as a response to imbalances between winds and form stresses through geostrophic adjustment. At equilibrium, there is sufficient mesoscale activity that the force balance of the layers are sustained by wind stress and form stresses, and no longer any need for meridional transport. Discrepancies between the wind stress and form stress profiles are associated with meridional eddy advection of zonal momentum, which also contribute to the maintenance of localised zonal jets.

Using parameters which characterise the Southern Ocean, we are able to reproduce transports comparable to the ACC and our solution shares several features with ACC observations, such as meandering jets and energetic mesoscale eddies. While the Southern Ocean is a dynamically complex system driven by both wind and buoyancy forcing, as well as interactions with adjacent ocean currents and unique topographic features such as Drake Passage, our results highlight the potential impact of mesoscale eddies on the ACC and emphasise the importance of resolving these small-scale features in ocean modelling studies of the Southern Ocean.

Acknowledgements

The authors thank Andrew Kiss and an anonymous reviewer for encouraging the investigation on the role of Rossby waves during spinup, and Bob Hallberg at GFDL for use of the GOLD isopycnal ocean model in this study. This work was supported by an Australian Research Council Grant (DP0877824), and numerical computations were conducted using the National Facility of the National Computational Infrastructure at ANU.

Appendix A. Derivation of interfacial form stress and energy transfer

Model results are numerical solutions to the Boussinesq isopycnal equations of motion,

$$\frac{\partial \boldsymbol{u}}{\partial t} + \boldsymbol{u}\cdot\nabla\boldsymbol{u} + f\hat{\boldsymbol{z}}\times\boldsymbol{u} + \nabla M = F \tag{A.1a}$$

$$\frac{\partial z_\rho}{\partial t} + \nabla\cdot(z_\rho\boldsymbol{u}) = 0 \tag{A.1b}$$

$$\frac{\partial M}{\partial \rho} = \frac{g}{\rho_0}z \tag{A.1c}$$

where $\boldsymbol{u}$ is the isopycnal velocity, M is the Montgomery potential, z_ρ is the isopycnal surface density, g is the gravitational acceleration, ρ_0 is the reference density, f is the Coriolis parameter, and F denotes any external (nonconservative) forcing, such as wind stress or bottom friction. We assume that there is no diapycnal transport. The isopycnal momentum density $z_\rho\boldsymbol{u}$ satisfies the equation

$$\frac{\partial}{\partial t}(z_\rho\boldsymbol{u}) + \nabla\cdot(z_\rho\boldsymbol{u}\boldsymbol{u}) + f\hat{\boldsymbol{z}}\times z_\rho\boldsymbol{u} + z_\rho\nabla M = z_\rho F \tag{A.2}$$

Using the layerwise decomposition discussed in Section 2, we integrate the momentum density Eq. (A.2) over each layer k to determine the layerwise momentum equation,

$$\frac{\partial}{\partial t}(h_k\boldsymbol{u}_k) + \nabla\cdot(h_k\boldsymbol{u}_k\boldsymbol{u}_k) + f\hat{\boldsymbol{z}}\times(h_k\boldsymbol{u}_k) + h_k\nabla M_k = h_kF_k. \tag{A.3}$$

Layer quantities can be interpreted as vertical averages across the layer, and any vertical shear or stratification within the layer has been neglected in the derivation of (A.3). The Montgomery potential is determined by a discretisation of the hydrostatic Eq. (A.1c), so that the layer Montgomery potentials are related by the equation

$$M_{k+1} = M_k + g_{k+\frac{1}{2}}\eta_{k+\frac{1}{2}}. \tag{A.4}$$

Each interfacial acceleration $g_{k+1/2}$ along $\eta_{k+1/2}$ is prescribed in the model, such as in Table 1, and corresponds to a buoyancy acceleration $g(\rho_{k+1}-\rho_k)/\rho_1$, where ρ_k is the density associated with layer k and g is the gravitational acceleration. The top layer Montgomery potential is $M_1 = p_1/2 + g_1/2\eta_1/2$, where $p_1/2$ is the atmospheric pressure and $g_1/2 = g$, although in this study we assume that $p_1/2 = 0$ and have used a reduced value of $g_1/2$ in order to slow the external gravity waves and permit a larger barotropic timestep.

The hydrostatic pressure $p_{k+1/2}$ (divided by the reference density ρ_1) along each interface $\eta_{k+1/2}$ is

$$\begin{aligned} p_{k+\frac{1}{2}} &= p_{\frac{1}{2}} + \sum_{l=1}^{k} g_{l-\frac{1}{2}}\left(\eta_{l-\frac{1}{2}} - \eta_{k+\frac{1}{2}}\right) = p_{\frac{1}{2}} + \sum_{l=1}^{k}\sum_{m=l}^{k} g_{l-\frac{1}{2}}h_m \\ &= p_{\frac{1}{2}} + \sum_{m=1}^{k}\sum_{l=1}^{m} g_{l-\frac{1}{2}}h_m \end{aligned} \tag{A.5}$$

This expression is simplified if we introduce the layer acceleration G_k, defined as

$$G_k = \sum_{l=1}^{k} g_{l-\frac{1}{2}}, \tag{A.6}$$

and corresponds to an acceleration $g\rho_k/\rho_1$. The interfacial pressures $p_{k+1/2}$ and Montgomery potentials M_k can then be related to each other by the equations

$$p_{k+\frac{1}{2}} = p_{k-\frac{1}{2}} + G_kh_k = M_k - G_k\eta_{k+\frac{1}{2}} = M_{k+1} - G_{k+1}\eta_{k+\frac{1}{2}}. \tag{A.7}$$

From these relationships, we can construct the Montgomery potential in terms of the interface pressures, so that

$$M_k = P_k + \frac{1}{2}G_k\left(\eta_{k-\frac{1}{2}} + \eta_{k+\frac{1}{2}}\right) \tag{A.8}$$

$$p_{k+\frac{1}{2}} - p_{k-\frac{1}{2}} = G_kh_k \tag{A.9}$$

where $P_k = \frac{1}{2}(p_{k-1/2} + p_{k+1/2})$.

In the momentum Eq. (A.3), the contribution by form stress is contained in the term $h_k\nabla M_k$. If we wish to describe the form stress in terms of the interfacial pressures, then this term becomes

$$
\begin{aligned}
h_k \nabla M_k &= h_k \nabla P_k + \frac{1}{2} G_k h_k \nabla\left(\eta_{k-\frac{1}{2}} + \eta_{k+\frac{1}{2}}\right) \\
&= \nabla(h_k P_k) - P_k \nabla h_k + \frac{1}{2}(G_k h_k)\nabla\left(\eta_{k-\frac{1}{2}} + \eta_{k+\frac{1}{2}}\right) \\
&= \nabla(h_k P_k) - \frac{1}{2}\left(p_{k-\frac{1}{2}} + p_{k+\frac{1}{2}}\right)\nabla\left(\eta_{k-\frac{1}{2}} - \eta_{k+\frac{1}{2}}\right) \\
&\quad - \frac{1}{2}\left(p_{k-\frac{1}{2}} - p_{k+\frac{1}{2}}\right)\nabla\left(\eta_{k-\frac{1}{2}} + \eta_{k+\frac{1}{2}}\right) \\
&= \nabla(h_k P_k) - p_{k-\frac{1}{2}} \nabla \eta_{k-\frac{1}{2}} + p_{k+\frac{1}{2}} \nabla \eta_{k+\frac{1}{2}} \qquad \text{(A.10)}
\end{aligned}
$$

so that the momentum equation becomes

$$
\begin{aligned}
&\frac{\partial}{\partial t}(h_k \boldsymbol{u}_k) + \nabla \cdot (h_k \boldsymbol{u}_k \boldsymbol{u}_k + h_k P_k \boldsymbol{I}) + f \hat{\boldsymbol{z}} \times (h_k \boldsymbol{u}_k) \\
&\quad = p_{k-\frac{1}{2}} \nabla \eta_{k-\frac{1}{2}} - p_{k+\frac{1}{2}} \nabla \eta_{k+\frac{1}{2}} + h_k F_k \qquad \text{(A.11)}
\end{aligned}
$$

which is Eq. (3) in Section 2. The first two terms on the right hand side are the form stresses across the upper and lower layers, respectively. We also note that

$$
h_k P_k = \int_{\eta_{k+\frac{1}{2}}}^{\eta_{k-\frac{1}{2}}} p(z)\, dz \qquad \text{(A.12)}
$$

where $p(z)$ is the hydrostatic pressure within a fluid column in the layer.

References

Anderson, D.L.T., Gill, A.E., 1975. Spin-up of a stratified ocean, with applications to upwelling. Deep Sea Res. 22, 583–596.

Colella, P., Woodward, P.R., 1984. The piecewise parabolic method (PPM) for gas-dynamical simulations. J. Comput. Phys. 54, 174–201.

Cunningham, S.A., Alderson, S.G., King, B.A., Brandon, M.A., 2003. Transport and variability of the antarctic circumpolar current in drake passage. J. Geophys. Res. 108, 8084.

Gill, A.E., Bryan, K., 1971. Effects of geometry on the circulation of a three-dimensional southern-hemisphere ocean model. Deep Sea Res. 18, 685–721.

Hallberg, R., 1995. Some aspects of the circulation in ocean basins with isopycnals intersecting the sloping boundaries. Ph.D. thesis, University of Washington.

Hallberg, R., 1997. Stable split time stepping schemes for large-scale ocean modeling. J. Comput. Phys. 135, 54–65.

Hallberg, R., Gnanadesikan, A., 2001. An exploration of the role of transient eddies in determining the transport of a zonally reentrant channel. J. Phys. Ocean 31, 3312–3330.

Hallberg, R., Gnanadesikan, A., 2006. The role of eddies in determining the structure and response of the wind-driven southern hemisphere overturning: results from the modeling eddies in the southern ocean (MESO) project. J. Phys. Ocean 36, 2232–2252.

Hidaka, K., Tsuchiya, M., 1953. On the antarctic circumpolar current. J. Marine Res. 12, 214–222.

Hogg, A.M., Blundell, J.R., 2006. Interdecadal variability of the southern ocean. J. Phys. Ocean 36, 1626–1645.

Hogg, A.M., Meredith, M.P., Blundell, J.R., Wilson, C., 2008. Eddy heat flux in the southern ocean: response to variable wind forcing. J. Climate 21, 608–620.

Hughes, C.W., 2002. Sverdrup-like theories of the antarctic circumpolar current. J. Marine Res. 60, 1–17.

Johnson, G.C., Bryden, H.L., 1989. On the size of the antarctic circumpolar current. Deep Sea Res. I 36, 39–53.

Karsten, R.H., Marshall, J., 2002. Constructing the residual circulation of the ACC from observations. J. Phys. Ocean 32, 3315–3327.

Killworth, P.D., Nanneh, M.M., 1994. Isopycnal momentum budget of the antarctic circumpolar current in the fine resolution antarctic model. J. Phys. Ocean 24, 1201–1223.

Lin, S.-J., Chao, W.C., Sud, Y.C., Walker, G.K., 1994. A class of the van Leer-type transport schemes and its application to the moisture transport in a general circulation model. Mon. Wea. Rev. 122, 1575–1593.

Lumpkin, R., Speer, K., 2007. Global ocean meridional overturning. J. Phys. Ocean 37, 2550–2562.

Marshall, J., Radko, T., 2003. Residual-mean solutions for the antarctic circumpolar current and its associated overturning circulation. J. Phys. Ocean 33, 2341–2354.

McWilliams, J.C., Holland, W.R., Chow, J.H.S., 1978. A description of numerical antarctic circumpolar currents. Dyn. Atmos. Oceans 2, 213–291.

Meredith, M.P., Hogg, A.M., 2006. Circumpolar response of southern ocean activity to a change in the southern annular mode. Geophys. Res. Lett. 33, L16608.

Munk, W.H., Palmén, E., 1951. Note on the dynamics of the antarctic circumpolar current. Tellus 3, 53–55.

Nadeau, L., Straub, D., 2009. Basin and channel contributions to a model antarctic circumpolar current. J. Phys. Ocean 39, 986–1002.

Olbers, D., 1998. Comments on the obscurant physics of 'form drag' in theorizing about the circumpolar current. J. Phys. Ocean 28, 1647–1654.

Olbers, D., Borowski, D., Völker, C., Wölff, J.-O., 2004. The dynamical balance, transport and circulation of the antarctic circumpolar current. Antarctic Sci. 16, 439–470.

Russell, J.L., Stouffer, R.J., Dixon, K.W., 2006. Intercomparison of the southern ocean circulations in IPCC coupled model control simulations. J. Clim. 19, 4560–4575.

Sadourny, R., 1975. The dynamics of finite-difference models of the shallow-water equations. J. Atmos. Sci. 32, 680–689.

Screen, J.A., Gillett, N.P., Stevens, D.P., Marshall, G.J., Roscoe, H.K., 2009. The role of eddies in the southern ocean temperature response to the southern annular mode. J. Clim. 22, 806–818.

Sokolov, S., Rintoul, S.R., 2007. Multiple jets of the antarctic circumpolar current south of Australia. J. Phys. Ocean 37, 1394–1412.

Stommel, H., 1957. A survey of ocean current theory. Deep Sea Res. 4, 149–184.

Straub, D.N., 1993. On the transport and angular momentum balance of channel models of the antarctic circumpolar current. J. Phys. Ocean 23, 776–782.

Tansley, C.E., Marshall, D.P., 2001. On the dynamics of wind-driven circumpolar currents. J. Phys. Ocean 31, 3258–3273.

Thompson, A.F., 2010. Jet formation and evolution in baroclinic turbulence with simple topography. J. Phys. Ocean 40, 257–278.

Treguier, A.M., McWilliams, J.C., 1990. Topographic influences on wind-driven, stratified flow in a β-plane channel: an idealized model for the antarctic circumpolar current. J. Phys. Ocean 20, 321–343.

Warren, B.A., LaCase, J.H., Robbins, P.E., 1996. On the obscurantist physics of "form drag" in theorizing about the circumpolar current. J. Phys. Ocean 26, 2297–2301.

Wolff, J.-O., Maier-Reimer, E., Olbers, D.J., 1991. Wind-driven flow over topography in a zonal β-plane channel: a quasi-geostrophic model of the antarctic circumpolar current. J. Phys. Ocean 21, 236–264.